Instability of the Stratified Ekman Boundary Layer and the Generation of Internal Waves[1,2]

Robert Kaylor and Alan J. Faller

Institute for Fluid Dynamics and Applied Mathematics and the Graduate Meteorology Program, University of Maryland, College Park 20742

(Manuscript received 6 October 1971, in revised form 28 December 1971)

ABSTRACT

With stable density stratification the shear-flow instability of the Ekman boundary layer exhibits two distinct regimes. At low values of a Richardson number the growth rate of instability, at specified Reynolds number, wavelength and angle, decreases linearly with Ri. At higher values of Ri the growth rate may decrease more slowly or may increase with Ri. The peculiar effects at the large values of Ri are interpreted as a resonance of the shear-flow instability with internal gravity waves. This resonance occurs when the speed of the shear-flow instability relative to the basic flow lies within the range of speeds of internal gravity waves relative to the basic flow, as determined by the Brunt-Väisälä frequency. Under these conditions the growth of waves appears to be dominated by the Type II mechanism of energy exchange for Ekman layer instability. Internal gravity waves generated by the shear-flow instability have their crests nearly parallel to the geostrophic flow above the boundary layer and move to the left of the geostrophic flow with speeds between approximately 0.15 and 0.7 times the geostrophic speed. The type II energy exchange mechanism with the apparent resonance is permitted by the Coriolis forces.

1. Introduction

Several experimental and theoretical studies have been concerned with the stability of the laminar Ekman boundary layer with neutral static stability and have found critical Reynolds numbers and other characteristics of the longitudinal roll vortices that occur at instability. Over a rigid boundary two distinct instability mechanisms occur, each tending to produce two-dimensional alternating helical rolls with horizontal axes but with different wavenumbers, different angles with respect to the basic flow, and different critical Reynolds numbers. Although two types of instability are found experimentally under suitable conditions, both instability mechanisms generally operate simultaneously, their relative importance being determined by the wavenumber and angle of the disturbance and the Reynolds number of the flow. In the case of experiments in circular geometry the Rossby number for the flow (Faller, 1963) also plays an important role.

The minimum critical Reynolds number for infinitesimal disturbances is $\mathrm{Re}_c \approx 55$ (Lilly, 1966; Tatro and Mollo-Christensen, 1967) where $\mathrm{Re} = U_g D/\nu$, U_g is the geostrophic flow above the boundary layer, $D = (\nu/\Omega)^{\frac{1}{2}}$ is the characteristic depth of the Ekman layer, Ω the angular speed of rotation of the coordinate system, and ν the kinematic viscosity. For the Ekman layer driven by wind stress on a water surface the critical value is $\mathrm{Re}_c \approx 12$ (Faller and Kaylor, 1967). This lower value is probably due to the fact that the cellular perturbations face a free surface rather than a rigid boundary even though the structure of the mean flow is identical in each case.

A stable density stratification will tend to suppress shear flow instabilities. But stable stratification also implies the possibility of internal gravity waves if a source of energy is provided in the proper frequency band. Normally an internal wave cannot directly draw upon the energy of shear flow but it is found here that if the frequency of an incipient shear-flow instability is close to the frequency of a possible internal gravity wave, this wave may be expected to amplify. A complementary view is that a moving shear-flow instability may achieve a phase relation between the density and the vertical velocity that is more characteristic of an internal wave than of ordinary cells forced upon a stably stratified fluid, and in such a case the stratification will not exert a strong damping influence. That such a process is possible has been shown in an earlier paper (Faller and Kaylor, 1967). We present here further calculations and evidence that the Ekman layer instability, although severely damped or nonexistent for moderate values of a Richardson number, may again amplify at greater values of Ri. The instability then

[1] The research reported herein was supported in part by the National Science Foundation under Grants GA-3443 and GA-4388.

[2] Contribution No. 036 from the Graduate Meteorology Program, University of Maryland, College Park.

takes a form more properly described as amplifying internal gravity waves rather than as amplifying longitudinal rolls.

In order to minimize the calculations and to simplify interpretation of the results, we have considered here only the laminar Ekman boundary layer for an incompressible fluid over a rigid boundary with a fixed statically stable vertical temperature gradient. The numerical calculations are lengthy and for the most part have been restricted to cases with Re=600, $H=H'/D=8.05$, where H' is the dimensional depth of fluid, and with the Prandtl number P=1. Other parameters have been restricted to limited ranges of interest. These parameters are the Richardson number, Ri, the angle of the two-dimensional disturbances with respect to the basic flow, ϵ, and the horizontal wavelength, $L=2\pi/l$, where l is the horizontal wavenumber.

Recent research by Brown (1972) has been concerned with the same general problem using a fundamentally different numerical approach. Although Brown omitted the Coriolis terms for simplicity of calculation (and therefore could not find the resonance with gravity waves), his results for the damping effect of stratification at the lower values of Ri are essentially in agreement with those found here.

2. The mathematical and numerical model

We assume a horizontally infinite flat layer of fluid of finite depth H' over a rigid plane boundary at $Z'=0$. The coordinate system is a right-handed Cartesian system X', Y', Z', with Z' positive upward normal to the plane boundary and counter to the direction of gravity $\mathbf{g}$. With the exception of a mean flow and perturbations, to be specified below, the fluid and the plane boundary are in constant angular rotation about the vertical axis with an angular velocity $\Omega=\mathbf{\Omega}\cdot\mathbf{k}$. Except for small perturbations the fluid is in hydrostatic balance and has a constant horizontal pressure gradient $\partial p'/\partial Y'$ with the corresponding geostrophic flow

$$U_g=-\frac{\alpha'}{2\Omega}\frac{\partial p'}{\partial Y'}$$

in the X' direction, and with a laminar Ekman spiral boundary layer flow. Primes refer to dimensional variables with α' the specific volume and p' the pressure.

We anticipate instability in the form of two-dimensional rolls at some angle ϵ with the X' axis, ϵ being positive for rotation in the same sense as $\mathbf{\Omega}$, i.e., toward the Y' axis. A new coordinate system x', y', z' is defined with the x' axis parallel to the axis of the rolls so that the two-dimensional perturbations are independent of x'. Since the value of ϵ for maximum instability is not known and will depend upon other parameters, ϵ itself becomes a parameter of the problem.

The Boussinesq approximation is employed and α' is taken to be linearly related to temperature. After forming a vorticity equation by the elimination of pressure from the y' and z' equations of motion and after appropriate nondimensionalization of the variables, the equations of motion and of heat transfer may be written (Faller and Kaylor, 1967):

$$\xi_t+\mathrm{Re}\,\mathrm{J}\left(\frac{\phi,\xi}{y,z}\right)-2u_z=\mathrm{Ri}\,\mathrm{Re}H\alpha_y+\nabla^2\xi, \tag{1}$$

$$u_t+\mathrm{Re}\,\mathrm{J}\left(\frac{\phi,u}{y,z}\right)+2\phi_z=-2\sin\epsilon+\nabla^2u, \tag{2}$$

$$\alpha_t+\mathrm{Re}\,\mathrm{J}\left(\frac{\phi,\alpha}{y,z}\right)=\mathrm{P}^{-1}\nabla^2\alpha, \tag{3}$$

where subscripts denote partial differentiation. In Eqs. (1)–(3) $\xi=w_y-v_z=\nabla^2\phi$ is the x component of vorticity, ϕ is a streamfunction in the y-z plane, and u, v and w are the x, y and z components of velocity. For nondimensionalization we have used the length scale $D=(\nu/\Omega)^{\frac{1}{2}}$, a velocity scale U_g, and a time scale Ω^{-1}. The apparent redundancy in the definition of a time scale independently of U_g and D is convenient and was justified in an earlier paper (Faller and Kaylor, 1966). Basically it means that nondimensional time is independent of Re (cf. Lilly, 1966) but the factor Re must be included when calculating advective speeds [cf. Eq. (8)]. The nondimensional perturbation specific volume is defined by

$$\alpha(y,z,t)=\frac{\alpha'(y,z,t)-\alpha_0'(z)}{\Delta\alpha_0'},$$

where $\alpha_0'(z)$ is the initially prescribed specific volume that varies linearly with z as given by

$$\alpha_0'=\tilde{\alpha}_0'+\Delta\alpha_0'[(z/H)-(1/2)].$$

Thus, $\tilde{\alpha}_0'$ is the value of α_0' at mid-depth, $z=H/2$, and is the reference value of α' used for the Boussinesq approximation. Finally, $\Delta\alpha_0'=\alpha_0'(H)-\alpha_0'(0)$ is the difference in α_0' between the upper and lower boundaries. These boundaries are assumed to be perfect thermal conductors.

The Reynolds number for the Ekman boundary layer is defined by $\mathrm{Re}=U_gD/\nu$ and the Richardson number for the problem is defined here by

$$\mathrm{Ri}=\frac{g\Delta\alpha_0'}{\tilde{\alpha}_0'H'}\Big/\left(\frac{U_g}{D}\right)^2.$$

The Prandtl number is $\mathrm{P}=\nu/\kappa$ with κ the thermal diffusivity; and J is the Jacobian operator.

In Eq. (2) the term $-2\sin\epsilon$ represents the x component of the horizontal pressure gradient which arises because of rotation of the axes through the angle ϵ. The

terms $2u_z$ and $2\phi_z$ in Eqs. (1) and (2), respectively, arise from the Coriolis accelerations. The steady-state solution of (1) and (2) with Re=0 is the Ekman spiral associated with geostrophic flow over a rigid boundary. For $H \gg 1$ the solution is well approximated by

$$U=(1-e^{-z}\cos z)\cos\epsilon+(e^{-z}\sin z)\sin\epsilon, \quad (4)$$

$$V=(e^{-z}\sin z)\cos\epsilon-(1-e^{-z}\cos z)\sin\epsilon, \quad (5)$$

$$W=0. \quad (6)$$

With the Ekman boundary layer there is no unique definition of a Richardson number because of the variable shear. However, since D is the characteristic thickness of the Ekman layer we have characterized the shear by U_g/D. This shear is the maximum value for each component of the flow (when $\epsilon=0°$) and this maximum shear occurs at the boundary. Therefore, our definition of Ri is compatible with that of Schlichting (1960) who used the shear at the boundary for consideration of the stability of the Blasius profile with stratification. (The limiting theoretical value for unstable flow was found by Schlichting to be Ri=1/24 above which the flow was stable for all Reynolds numbers.)

By using the maximum shear our values of Ri are much lower than values representative of the shear in the boundary layer as a whole. If the depth πD is regarded as a more appropriate depth for the estimation of an average shear, our values of Ri should be multiplied by $\pi^2 \approx 10$. Many studies of shear flow instability have used a local Richardson number evaluated at an inflection point. Brown (1972) has pointed out that for his studies a local value of Ri, associated with the inflection point at angle ϵ, appears to be appropriate. From Eq. (5) the nondimensional shear at the first inflection point above $z=0$ is $\partial V/\partial z_i=\exp\{-[(\pi/2)-\epsilon]\}$, and the local Richardson number is given by $\mathrm{Ri}_l=\exp\{2[(\pi/2)-\epsilon]\}\,\mathrm{Ri}$. At $\epsilon=0$ this factor is 23.2

The numerical calculations were carried out at fixed intervals $\Delta\mathrm{Ri}=0.001553$. For ease of reference the calculations will be described in terms of a nominal Richardson number Ri_n for which $\Delta\mathrm{Ri}_n=1$. Table 1 allows a conversion from one definition to another including Ri_l at $\epsilon=0$.

The Brunt-Väisälä frequency, a characteristic of the stratification, may be defined as $N' \equiv (g\Delta\alpha'_0)/(\tilde{\alpha}_0' H')$. The corresponding nondimensional frequency is $N=N'/\Omega=\mathrm{Re}(\mathrm{Ri})^{\frac{1}{2}}$. The nondimensional frequency of an internal gravity wave of horizontal wavelength L and vertical wavelength Z for a nondiffusive fluid is then given by[3]

$$\omega_g=\left[1+\left(\frac{Z}{L}N\right)^2\Big/1+\left(\frac{Z}{L}\right)^2\right]^{\frac{1}{2}}. \quad (7)$$

In the special case of the gravest mode in the vertical for inviscid but rigid boundaries, $Z=2H$. The horizontal phase speed of an internal wave corresponding to (7) is

$$c_g=(\omega_g L)/(2\pi\,\mathrm{Re}). \quad (8)$$

[3] For the theory leading to Eq. (7) see Eckart (1960), p. 143.

TABLE 1. A comparison of Richardson numbers.

Nominal Richardson number Ri_n	Richardson number using shear (U_g/D) Ri	Total Ekman layer Richardson number using shear $(U_g/\pi D)$ $\pi^2\mathrm{Ri}$	Local Richardson number at the inflection point $(\partial^2 V/\partial z^2=0)$ for $\epsilon=0$, $\mathrm{Ri}_l=e^{\pi}\mathrm{Ri}$
1	0.00155	0.0153	0.0359
2	0.00312	0.0307	0.0723
3	0.00466	0.0460	0.1080
4	0.00621	0.0613	0.1440
5	0.00776	0.0766	0.1799
6	0.00932	0.0920	0.2161
8	0.01242	0.1226	0.2879
12	0.01883	0.1839	0.4366
16	0.02484	0.2452	0.5685

Details of our numerical methods have been presented in earlier publications (Faller and Kaylor, 1966, 1967). For this study the dependent variables were separated into mean and perturbation components and the mean flow and stratification were held constant. The perturbations were expressed as a Fourier series in y and each mode in y was considered independently, neglecting interactions, i.e., the equivalent of linearized perturbation theory. A vertical grid spacing Δz was chosen and a finite-difference solution for the undisturbed Ekman boundary layer in the finite depth H was calculated for no-slip conditions, $u=v=w=0$, at the bottom boundary and rigid free-slip conditions at $z=H$, $u_z=v_z=w=0$.

The perturbations for each horizontal mode were then functions of z and t. Each calculation was started with some more or less arbitrary initial perturbation or with the final results of some previous calculation. For each case the parameters to be chosen were Re, Ri, P, H, L and ϵ plus the numerical parameters Δz and Δt, but to minimize the variables we fixed Re=600, P=1 and $H=8.05$. In the present series of experiments the Euler-implicit time step was used with the number of iterations at each step determined by a simple criterion for the convergence of the solution. Usually only one or two iterations were required. For each wave the solution of the one-dimensional Poisson equation to obtain ϕ from ξ at each step was obtained by the use of Thomas' algorithm for the solution of a tri-diagonal matrix. Further details of the numerical methods may be found in the references cited above.

Using the initial-value approach outlined above a wide variety of vertical modes may be introduced by the initial perturbation. But, usually, if there is an instability of the flow, other modes will decay to relatively small amplitudes while the amplifying mode grows. After some time the total energy of the flow is dominated by the amplifying mode or by the most unstable mode if more than one unstable mode exists.

The growth rate of total energy is called $2k$. (Correspondingly, if only a single mode exists its growth rate of amplitude is k as used by the authors in referenced publications.) When $2k$ attains a sufficiently constant value over a long period it is assumed that a single mode, either amplifying or decaying, dominates the circulation. If all modes are damped this procedure singles out the most slowly decaying mode, and in the case of a simple shear-flow instability this usually corresponds closely to that mode that would be unstable if the Reynolds number were increased to its critical value.

Difficulties associated with the stable stratification sometimes arise in the use of this initial-value method. Various internal gravity waves generated by the initial perturbation may progress in either the positive or negative y direction. Of these the gravest modes decay rather slowly. Therefore, a long calculation may be required to separate a slowly growing unstable mode from a slowly decaying gravity wave, the length of the required calculation being dependent upon the ratio of their initial amplitudes. In the case of no instability the cellular motions that would be unstable at a slightly larger value of Re may decay more rapidly than the gravest internal wave. Then the negative growth rate that is obtained is that of the internal wave and is not useful for the determination of a neutral curve by interpolation as is the case without density stratification. Fig. 1 is an example of the time dependence of $2k$ for three values of L. By the time $t=2.0$ patterns of steadily damping oscillations of growth rate have emerged, and after $t=4.0$ quite reliable extrapolated values may be obtained.

3. Numerical results at $\varepsilon=0$

The principal physical phenomena implied by all calculations are best illustrated by a series of numerical experiments in which only Ri (or equivalently N) was varied. The other parameters were fixed at Re=600, $H=8.05$, P=1, $L=24$ and $\epsilon=0$. By way of introduction Fig. 2 illustrates the patterns of u, α and ϕ in the y-z plane for steady growth of $2k=13.3$ at $\mathrm{Ri}_n=0$. In this example α is carried in the calculation as a passive tracer and has no influence upon the cellular motions as may be inferred from Eqs. (2) and (3).

Fig. 3 presents the growth rate of energy $2k$ and the phase speed c for several values of Ri_n. For $\mathrm{Ri}_n<3$, $2k$ decreases linearly with Ri_n and neutral stability is indicated at $\mathrm{Ri}_n\approx 2.5$. The numerical results at $\mathrm{Ri}_n=3$ show steady decay of a gravity wave with $2k=-0.7$, thus implying that low-level cellular perturbations similar to those of Fig. 2 decayed at a more rapid rate. But for $\mathrm{Ri}_n>3$ positive growth again occurred, to the limit of our computations at $\mathrm{Ri}_n=16$.

In Fig. 3 the values of phase speed c are compared with the speeds of internal gravity waves from (8) on the basis of different assumptions about Z. The curve c_N is the phase speed that corresponds to $Z\to\infty$ and $\omega_g=N$, while c_H corresponds to the gravest normal mode with $Z=2H$ and $L=24$. [The remaining curve c_α was determined from Eq. (8) by measuring the vertical wavelength of α cells in the various computations as described below.] From Fig. 3 it appears that with $c>c_N(\mathrm{Ri}_n<3)$ the stratification has a strong damping effect, but when $c\leqslant c_N(\mathrm{Ri}_n>3)$ the effect of the stratification is minimized and instability is again allowed. This behavior suggests resonance of the shear flow instability with internal gravity waves at the larger values of Ri_n.

Fig. 4 illustrates the cellular patterns of α and ϕ for three characteristic values of Ri_n: the linearly damped region ($\mathrm{Ri}_n=1$), the totally damped region ($\mathrm{Ri}_n=3$), and the resonant region ($\mathrm{Ri}_n=12$). Panels (a) and (b) show patterns very similar to the case for $\mathrm{Ri}_n=0$ (Fig. 1). The fully damped case [panels (c) and (d)] shows only high-level cells exactly in phase. Cells initially centered in the lower levels damped out rapidly leaving only a slowly decaying internal gravity wave that was restricted to the upper levels because of the shear flow in the Ekman layer. Although internal waves progressing in both the positive and negative y directions are possible, and were included in the initial perturbation, it appears that waves progressing in the positive direction are more strongly coupled to the Ekman layer and damp more rapidly. Thus, the residual wave had $c<0$ compared to $c>0$ for the two examples with amplification. This difference accounts for the opposite phase relation between α and ϕ at $\mathrm{Ri}_n=3$. In panel (c) the quarter vertical wavelength of the α cells is $Z/4=3$, from the cell center to the upper boundary.

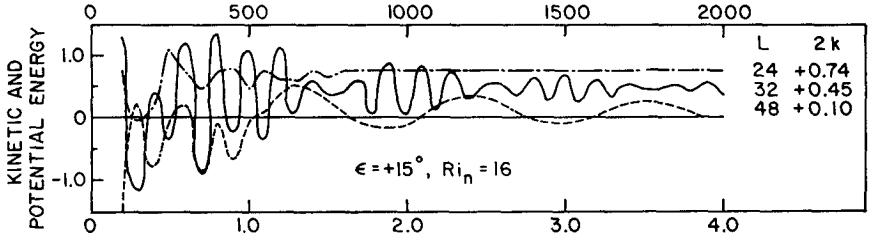

FIG. 1. Typical curves of the growth rate of energy $2k$ (ordinate) vs time (abscissa) in radians (lower scale) and time steps (upper scale). Extrapolated values of $2k$ for each value of L are given on the right. The apparent modulation for $L=32$ is an aliasing effect due to computer printout limited to every 50 time steps.

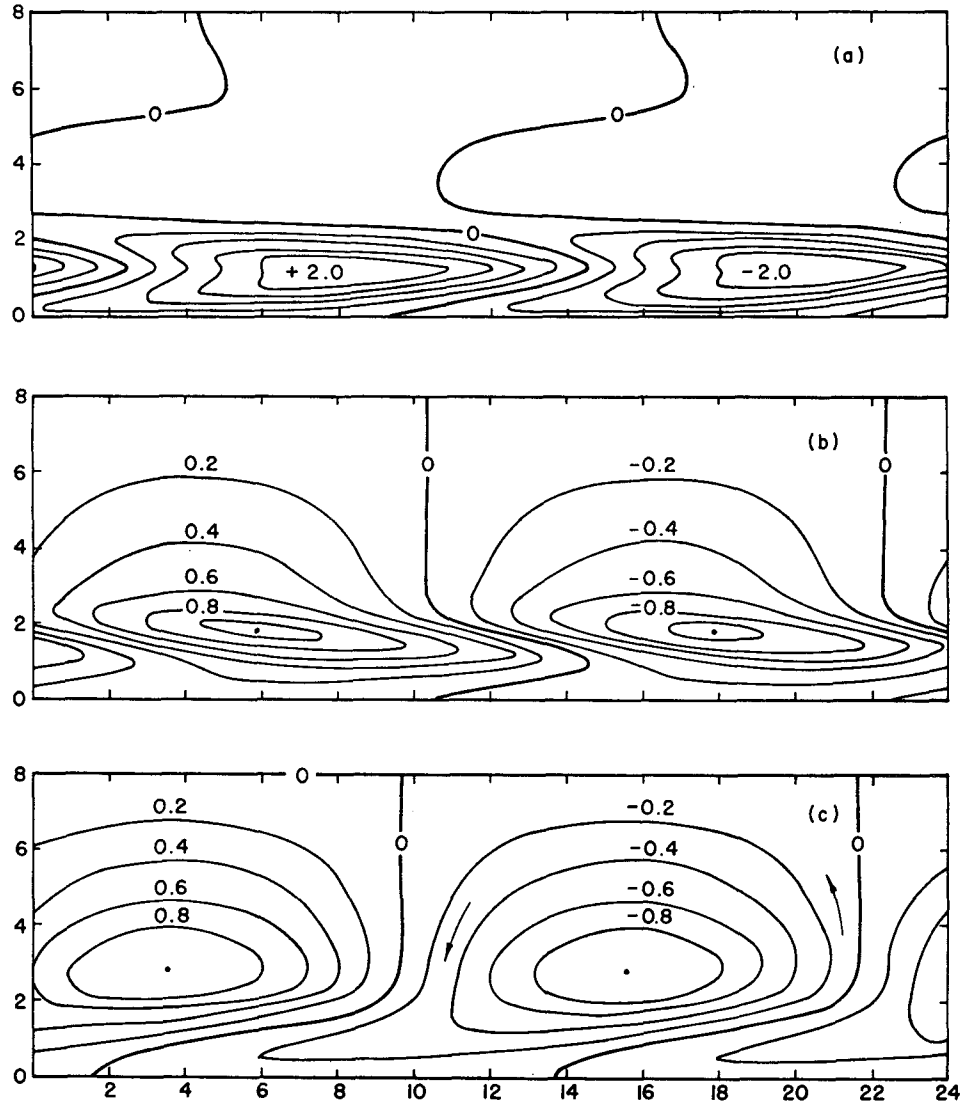

FIG. 2. The patterns of u(a), α(b), and ϕ(c) for Ri=0 and for Re=600, $H=8.05$, $L=24$, $\epsilon=0$, P=1. In this calculation α has no influence upon the circulation and is carried only as a passive tracer. Arrows in (c) indicate the direction of cellular circulation.

The corresponding gravity wave speed from (8) is $c_\alpha=-0.116$, nearly precisely the speed determined from successive time steps in the numerical computation, $c=-0.117$.

In the resonant region at $\mathrm{Ri}_n=12$ [panels (e) and (f)] cells (or waves) occur once again at the lower levels. The cells in α and ϕ are almost exactly in phase above $z=1.5$ and move with $c>0$. The interpretation is one of cells generated by the shear flow in the lower levels and feeding an internal gravity wave at upper levels. Above $\mathrm{Ri}_n=3$ the phase speed is determined by some combination of the shear flow instability and internal wave propagation. Again using the upper half of the α cells to estimate a value for Z, we have $Z/4=6.5$ in this case. The values c_α in Fig. 2 have been determined in this manner. At $\mathrm{Ri}_n=16$ the curves of c_α and c appear to approach each other indicating the dominance of the wave propagation effect at larger Ri_n.

If overturning cells are superimposed upon a stable, thermally stratified fluid, a downward heat flux proportional to the product $-\overline{w\alpha}$ is to be expected, the bar indicating an average over the wavelength L. Noting that $w=\phi_y$, it follows that for periodic variations of ϕ and α the downward flux is proportional to $-\overline{w\alpha}=\Phi A(\pi r/L)$, where ϕ and α have been represented by $\phi=\Phi\sin(ly-\beta)$ and $\alpha=A\sin(ly-\gamma)$. The factor r, given by $r=\sin(\gamma-\beta)$, is the negative of the correlation coefficient between w and α. The phase difference $(\gamma-\beta)$ between ϕ and α (or the correlation r) at any level is indicative of the sense and efficiency of the vertical convection of heat. If ϕ and α are 90° out of phase, so that $\gamma-\beta=\pi/2$, w and α are 180° out of phase and the

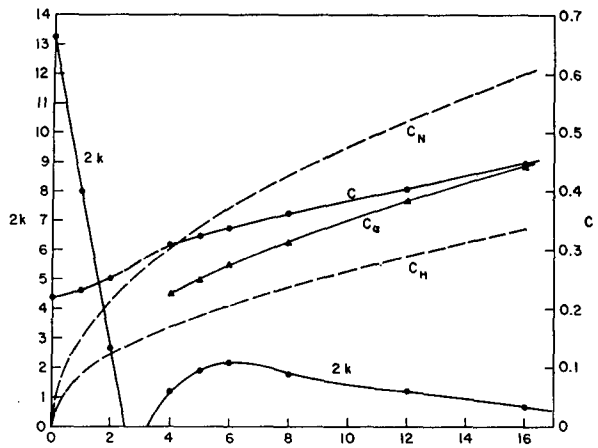

FIG. 3. Growth rates of energy (left ordinate) and phase speeds (right ordinate) as a function of Ri_n (abscissa): c_N, c_H and c_α are theoretical speeds of internal gravity waves based upon different assumptions about the vertical scale of the internal waves. All parameters other than Ri_n were held constant at Re=600, $L=24$, $\epsilon=0$, $H=8.05$, P=1.

downward heat transport is a maximum with $r=1$. On the other hand, simple internal gravity waves are characterized by $r=0$ with no convective heat transport. Fig. 5 gives some details concerning the relative distributions of ϕ and α, in addition to those of Fig. 4, that relate to the question of the convective heat flux.

The solid curves of Figure 5 (shaded areas) give values of r vs z for selected values of Ri_n. Positive values of r indicate the expected downward heat flux. Some negative values occur at $\mathrm{Ri}_n=2$ and $\mathrm{Ri}_n>8$ at the lower levels. At these levels the heat flux due to the perturbations is upward, along the temperature gradient, and if an eddy heat transfer coefficient were defined it would have negative values where $r<0$. These negative values result from a forced phase relation between α and ϕ associated with advective effects in the Ekman layer.

For cells superimposed upon a stably stratified fluid one might at first expect a phase difference of 90° between α and ϕ with $r=1$. But at $\mathrm{Ri}_n=0$, where α is but a passive tracer, the small calculated value $r=0.19$ for $z>2$ arises from the rapid movement of the ϕ cells. [Nearly stationary patterns occur near $\epsilon=15$ (see Table 2) but even then only a small phase angle difference should be expected because of the component of the geostrophic flow normal to the cells.] This rapid movement of cells relative to the flow above the boundary layer is an essential ingredient of the suggested resonance mechanism.

Near $\mathrm{Ri}_n=0$ we see from Fig. 3 that $\partial c/\partial\,\mathrm{Ri}_n>0$. From Fig. 5 above $z=2$ there is a corresponding decrease in r associated with the increased phase speed. These changes with Ri_n apparently represent an accommodation that reduces the damping effect of the stratification. The appearance of values $r<0$ at $\mathrm{Ri}_n=2$ at low levels also corresponds to reduced damping effects. But this phase speed and phase angle accommodation is limited and for this series of computations it is gradually overcome by the increasing stable stratification (increasing Ri_n) as long as $c<c_N$. But when $c\geqslant c_N$, $r=0$ at upper levels ($z>2$) and the damping at lower levels ($z<2$) is insufficient to suppress the instability.

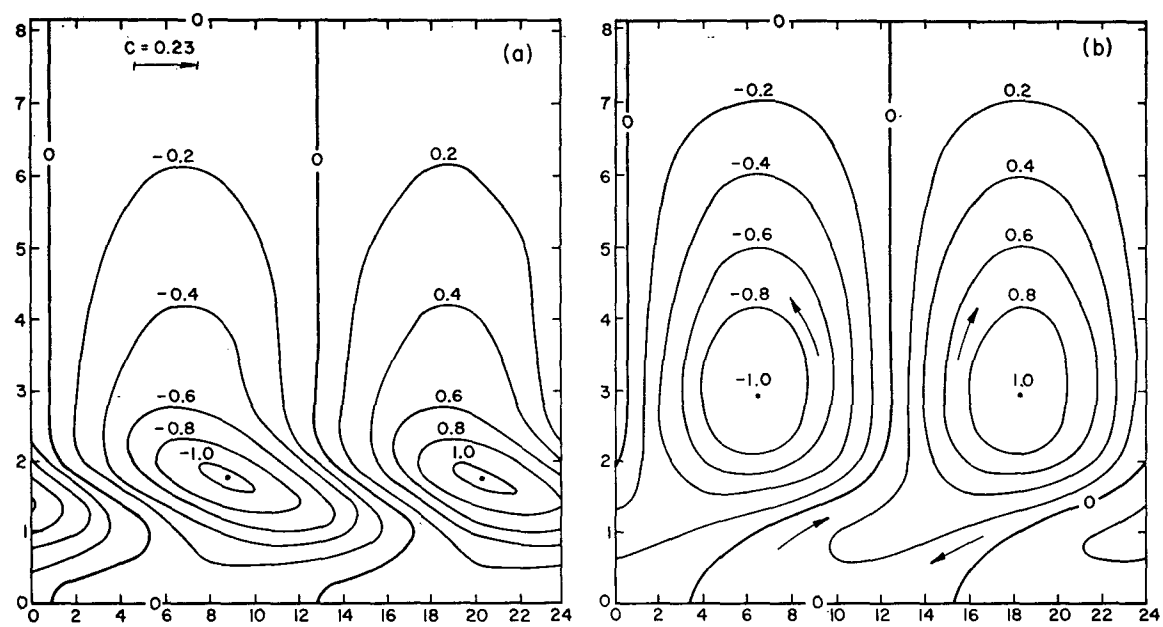

FIG. 4. Patterns of α and ϕ in the y-z plane for $\mathrm{Ri}_n=1$ [(a) and (b)], $\mathrm{Ri}_n=3$ [(c) and (d)], and $\mathrm{Ri}_n=12$ [(e) and (f)]. At $\mathrm{Ri}_n=3$ the cellular patterns represent slowly decaying internal gravity waves cut off in the lower levels by the shear of the Ekman layer. All parameters are the same as for Fig. 3.

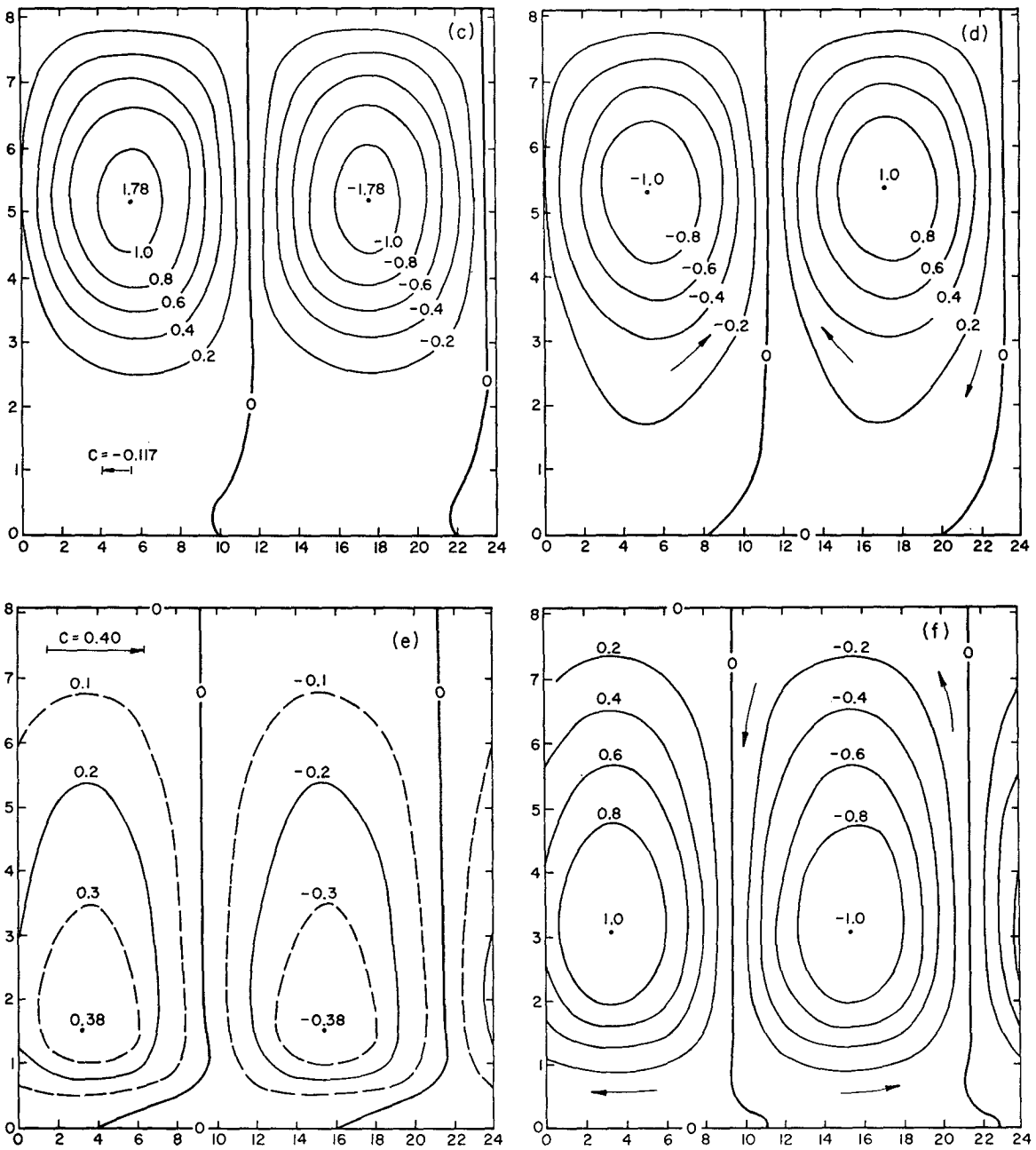

FIG. 4. (*continued*).

4. The energy cycle

Eqs. (1)–(3) may be transformed to a compatible set of energy equations by multiplying by ϕ, u and $\mathrm{Ri}H^2\alpha$, respectively, and by integrating over y from 0 to L and over z from 0 to H. The resultant equations may be written:

$$E_t=\frac{1}{A}\int \underbrace{(-\mathrm{Re}uwU_z}_{\mathrm{II}}\underbrace{+2uv}_{-\mathrm{III}}\underbrace{+u\nabla^2u)}_{-\mathrm{V}}dA, \tag{9}$$

$$K_t=\frac{1}{A}\int \underbrace{(\mathrm{Re}\,\mathrm{Ri}H\alpha w}_{-\mathrm{IV}}\underbrace{-2uv}_{\mathrm{III}}\underbrace{+\mathrm{Re}Vwv_z}_{\mathrm{I}}\underbrace{-\xi^2)}_{-\mathrm{VI}}dA, \tag{10}$$

$$P_t=\frac{1}{A}\int \underbrace{(-\mathrm{Re}\,\mathrm{Ri}H\alpha w}_{\mathrm{IV}}\underbrace{+\mathrm{Ri}H^2P^{-1}\alpha\nabla^2\alpha)}_{-\mathrm{VII}}dA, \tag{11}$$

where

$$K=(1/A)\int[(v^2+w^2)/2]dA$$

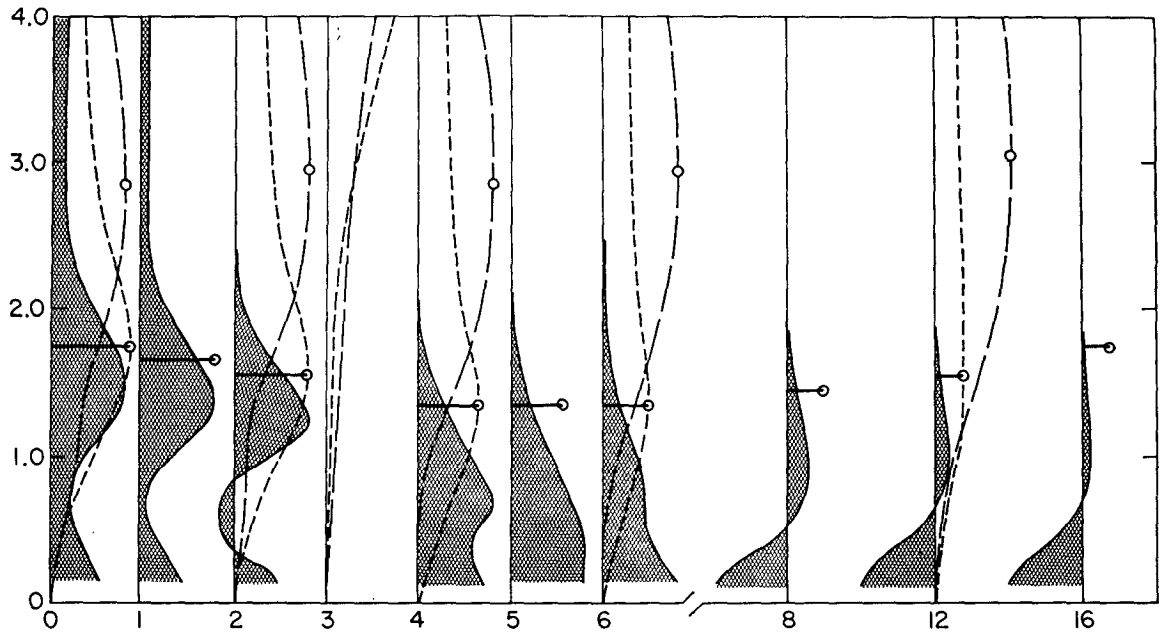

FIG. 5. Values of the correlation r (solid lines, shaded areas), ϕ amplitudes Φ (long dashes), and α amplitudes A (short dashes), as functions of Ri_n (abscissa) and z (ordinate). Maximum values of Φ are indicated by circles and maxima of A by barred circles. The maximum values of Φ are normalized to unity and provide the scale for A and R. Note that only the lower half of the fluid layer is represented. All parameters are the same as for Fig. 3.

is the overturning kinetic energy of the rolls,

$$E=(1/A)\int (u^2/2)dA$$

is the longitudinal kinetic energy, and

$$P=(1/A)\int \mathrm{Ri}H(\alpha^2/2)dA$$

is the potential energy of the rolls. The indicated terms in Eqs. (9)–(11) are as follows

I: the rate of generation of K from the basic cross flow $V(z)$ [see Eq. (5)]

II: the rate of generation of E by the action of cells upon the basic longitudinal flow $U(z)$ [see Eq. (4)]

III: the rate of transfer of energy from E to K by the action of the Coriolis forces

TABLE 2. Growth rates of energy $2k$ and phase speeds c for selected values of L, ϵ and Ri_n.

		$L=8$		$L=12$		$L=24$		$L=48$	
Ri_n	ϵ	$2k$	c	$2k$	c	$2k$	c	$2k$	c
	45			9.7	−0.268	7.8	−0.226		
	30	0.1	−0.162	23.7	−0.153	15.6	−0.106	2.9	−0.056
	15	18.1	−0.014	29.2	−0.005	18.1	0.039	5.9	0.092
0	0	7.3	0.165	17.9	0.176	13.3	0.216	6.1	0.266
	−15	−2.9	0.405	7.8	0.403	7.1	0.427	4.4	0.460
	−30			5.8	0.610	4.8	0.633	2.6	0.658
	−45			3.5	0.792	3.0	0.812	1.7	0.833
	−60			1.8	0.931	1.8	0.949	1.2	0.966
	45			0.6	−2.50				
	30			8.0	−1.30			−0.3	0.044
	15			−0.9	0.23	1.1	0.160	2.0	0.211
8	0					1.8	0.362	1.6	0.410
	−15					1.2	0.581	1.0	0.625
	−30					0.6	0.793	0.7	0.832
	−45					0.2	0.979	0.4	1.105
	−60							0.06	1.154
	+30					(—)		(—)	
	+15					0.73	0.234	0.10	0.301
16	0					0.70	0.446	0.45	0.509
	−15					0.42	0.669	0.39	0.726
	−30					0.14	0.884	0.20	0.935

IV: the rate of transfer from K to P due to the cellular correlation of α and w

V, VI, VII: the rates of dissipation of E, K and P, respectively.

Terms I and II may be characterized as transfers from the basic flow, while terms III and IV are transfers between the different components of energy E, K and P. Schematic diagrams of these transfers are given in Fig. 6.

It is convenient to discuss the energy cycle in relation to the two instability mechanisms of the Ekman boundary layer. Type I, the common inflectional instability, is represented by term I which involves the profile of $V(z)$ and which directly contributes to the growth of K. The Type II instability was clearly identified as a different mechanism by Lilly (1966) who referred to it as the "parallel mode" instability. Term II is the primary source for the Type II instability, but term III, which arises from the Coriolis forces, is also an essential element of this mechanism. Energy introduced into E by term II must be transferred from E to K by term III in order to maintain cellular overturning motions. In turn, the cells must be present in order to tap the source of energy available from the mean flow $U(z)$ through term II. It is apparent from Eqs. (9) and (10) that without the transfer term from the Coriolis effect the energy introduced into E by term II could not be utilized to maintain cellular motions.

Although this latter type of mechanism came clearly to light in consideration of the Ekman boundary layer, it was anticipated by Burgers (1953) in a discussion of possible longitudinal vortices in turbulent boundary layers. He introduced energy-conserving terms, quite analogous to the Coriolis terms, into a set of model equations of motion of a fluid in order to represent effects possibly introduced by the complex interactions of smaller scale turbulence. In addition, the symmetric baroclinic instability studied by Stone (1966) and the "instability of the thermal wind" studied by Faller and Kaylor (1969) utilize the same basic energy transfer, but in these latter studies the basic shear was taken to be constant and a mean stratification was superimposed.

In Fig. 6 the dashed arrows indicate the role of the cells (i.e., of K) in term II. As shown before, the case $\mathrm{Ri}_n=3$ is anomalous and separates two distinct regimes of flow. Thus, for $\mathrm{Ri}_n<3$, the dominant source of K is term I, while for $\mathrm{Ri}_n>3$ the transfer term III, associated with the Type II mechanism, exceeds term I. For $\mathrm{Ri}_n<3$ almost all terms and the values of E, K and P vary with Ri_n in a nearly linear fashion. In particular, the linear decrease of term I with increasing Ri_n shows that when this term approaches 0 (near $\mathrm{Ri}_n=3$) the instability is destroyed. This occurs even though term II decreases with Ri_n relatively slowly and even though term III increases with Ri_n. Thus, it appears that for these values of the parameters and for $\mathrm{Ri}_n<3$

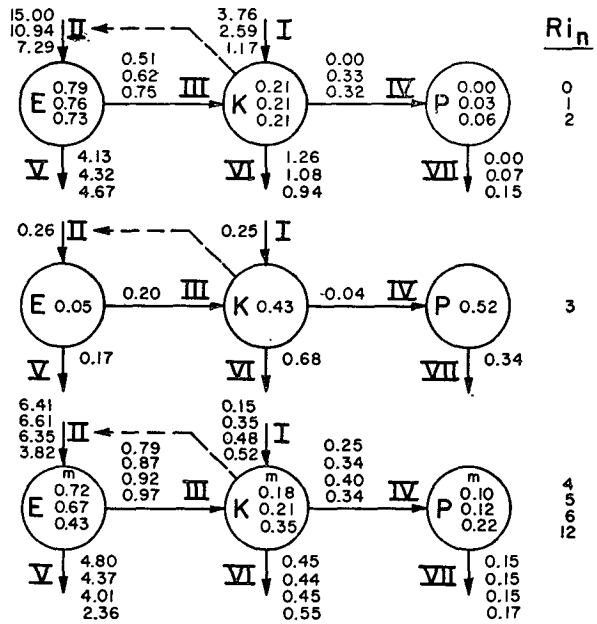

FIG. 6. Schematic energy diagrams for E, K and P and for the rates of transfer (terms I–VII for several values of Ri_n). In each case all values have been normalized by the total energy $\Sigma=U+K+P$. The dashed arrow emphasizes the effect of existing cells upon the source term II. [Values for U, K and P at $\mathrm{Ri}_n=4$ are missing (m).] All parameters are the same as for Fig. 3.

the Type I mechanism is dominant even though term II is about four times larger than term I and contributes greatly to the sum $E+K$.

For the nearly pure internal wave at $\mathrm{Ri}_n=3$ the potential and kinetic energies are nearly equal and there is very little transfer between them (term IV). Above $\mathrm{Ri}_n=3$ the relative values of P and K increase steadily as the perturbations take on more the character of internal waves.

5. Calculations other than at $\epsilon=0$

Numerical results at values of ϵ and L other than 0 and 24, respectively, bear out the conclusion that resonance with gravity waves allows instability at values of Ri larger than might otherwise be expected. To illustrate this point we now compare the actual results of our computations with the results that would be expected in the absence of a resonance mechanism.

Fig. 7 shows some typical results for the growth rate $2k$ vs Ri_n for $L=12$ and for $\epsilon=15$, 30 and 45. As with the computations at $L=24$ and $\epsilon=0$, the growth rate in each case decreases linearly with Ri, although with slopes and intercepts dependent upon ϵ and L. These results are characteristic of conditions where resonance cannot occur. Therefore, it is assumed that this linear decrease of growth rate with stable stratification is what should normally be expected when cells (or turbulence) are forced upon a stably stratified fluid. It is assumed that the linear response to Ri, as graphically

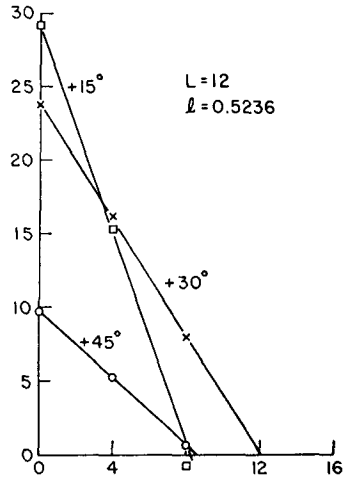

FIG. 7. Examples of the linear decrease of growth rate $2k$ with Ri_n at low values of Ri_n. Although slopes and intercepts vary with the several parameters of the problem, a linear decrease of $2k$ with Ri_n prevails as long as $c > c_N$.

displayed in Fig. 7, would continue to large negative values (decay) at higher Ri if the resonance mechanism were not available. On this basis the relative significance of resonance is well illustrated by a comparison of the actual computational results with the results that would be anticipated without resonance.

Fig. 8 illustrates neutral curves in an $\epsilon - L$ diagram for various values of Ri_n *under the assumption of a linear decrease of 2k with Ri.* Neutral stability points from which the curves were drawn were obtained from data like those of Fig. 7. For example, in Fig. 7 the intercept of the $\epsilon = 30$ line with the axis of the abscissas is at $\mathrm{Ri}_n = 12$ and provides one point of neutral stability for Fig. 8 at $\epsilon = 30$ and $\mathrm{Ri}_n = 12$. [It is important to note that Figs. 8 and 9 are not growth rate diagrams as used by Lilly (1966).] The extrapolated maximum value of Ri_n for instability in this case would be $\mathrm{Ri}_n \approx 13$ at $\epsilon = 35$ and $L = 12$.

Fig. 9 shows the actual neutral curves based upon an extrapolation of all calculated growth rates. The resonance is seen to affect primarily those waves that have a significant speed in the positive y direction, to the left of the direction of the geostrophic flow. Values of secondary maxima of growth rate of energy as given in Fig. 9 suggest a maximum Ri_n for instability near $\mathrm{Ri}_n = 20$, $\epsilon = 10$, and $L = 24$, but this result applies only for our selected values of the other parameters, principally $\mathrm{Re} = 600$.

It is not convenient to plot phase speed and growth rates in Figs. 8 and 9 because c and $2k$ are functions of Ri as well as of ϵ and L. Table 2 lists values of c and $2k$ for representative values of Ri, ϵ and L at which computations were made.

In the interpretation of Fig. 9 it should be noted that neutral curves in the interval $0 < \mathrm{Ri}_n < 4$ do not progress smoothly by interpolation between the 0 and 4 lines of the figure. The mark at $\epsilon = 0$ and $L = 24$ in Figs. 8 and 9

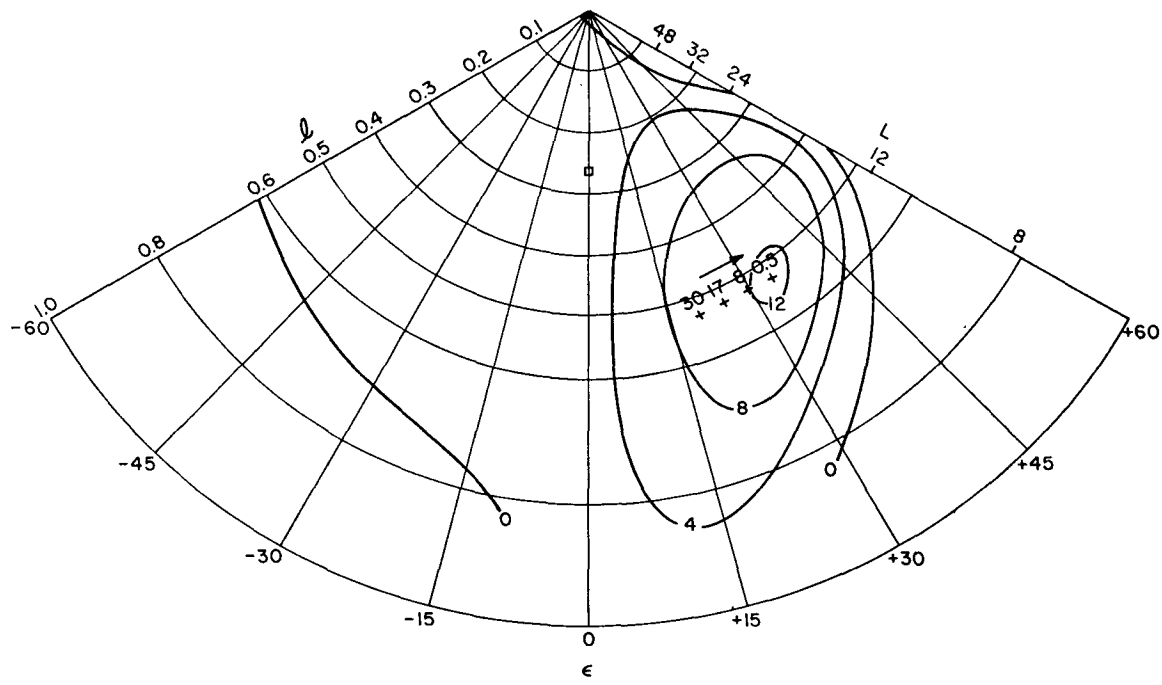

FIG. 8. Interpolated lines of neutral stability for several values of Ri_n based upon the assumption of a linear decrease of growth rate with Ri_n (see Fig. 7). The corresponding maximum values of $2k$ are indicated. The arrow shows the direction of increasing Ri_n (from 0 to 12) for the growth rate maxima. The square at $L = 24$ and $\epsilon = 0$ refers to the computations illustrated in Figs. 3–6.

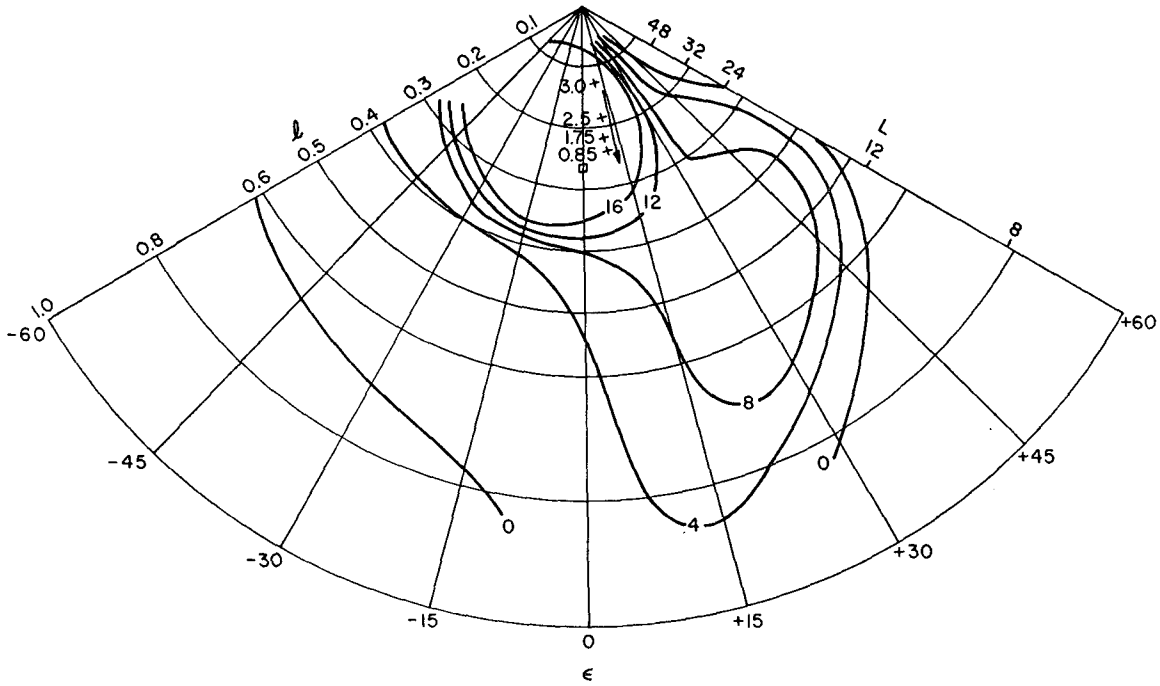

FIG. 9. Interpolated lines of neutral stability for several values of Ri_n from numerical calculations (compare with Fig. 8). The secondary maxima of $2k$ for $Ri_n=4$, 8 and 12, and the maximum for $Ri_n=16$ are indicated in that order by the arrow.

corresponds to the series of data in Fig. 3 which indicates stability in the approximate interval $2.5<Ri_n<3.3$. Therefore, a neutral curve for $Ri_n=3$ in Fig. 9 would exclude the point at $\epsilon=0$ and $L=24$. We do not have a sufficient number of calculations to draw the intermediate neutral curves for small Ri_n.

Fig. 10 is a comparison of the growth rate curves for the two values $Ri_n=0$ and $Ri_n=2.55$ as a function of ϵ for $Re=600$, $L=24$ and $H=11.4$. These calculations confirm the existence of the decay region of Fig. 3 near $Ri_n=3$ even though the conditions are slightly different ($Ri_n=2.55$, $H=11.4$) and the calculations were made with a different numerical program. The shaded area of Fig. 10b, indicating the region of possible internal gravity waves, is determined from the relation

$$(-\sin\epsilon-c_N)<c<(-\sin\epsilon+c_N), \qquad (12)$$

where $-\sin\epsilon$ is the y component of the geostrophic flow. Although the lower level flow in the Ekman layer would have some influence, it is presumed that the y component of flow above the boundary layer would have the predominant advective effect upon deep cells. Fig. 10b then shows that amplification at negative ϵ is allowed when the speed of the disturbance lies within the interval of relation (12).

In Fig. 3 a dashed line has been used to connect calculations of c at $Ri_n=2$ and $Ri_n=4$, thus implying some degree of continuity in c despite the fact that decaying modes occur for $2.5<Ri_n<3.3$. Also, as shown in Section 4 and in Fig. 6, the energy change for $Ri_n<3$ is significantly different than for $Ri_n>3$ suggesting that

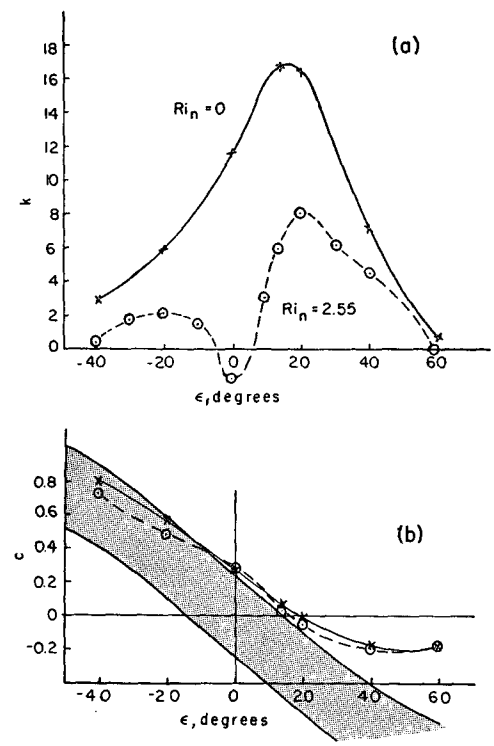

FIG. 10(a). Growth rates of amplitude vs ϵ for $Ri_n=0$ and $Ri_n=2.55$, for $Re=600$, $H=11.4$, $L=24$, and $P=1$. The secondary maximum for $Ri_n=2.55$ at negative ϵ indicates resonance with internal waves. 10(b). Phase speeds c at $Ri_n=0$ and $Ri_n=2.55$ vs ϵ. The shaded area includes the possible speeds of internal gravity waves [adapted from Faller and Kaylor (1967)].

there is a real discontinuity in the eigenfunctions across the region of decay. On the other hand, the extension of the low Ri_n curve seems to be a natural one, and at certain wavelengths and angles other than at $L=24$ and $\epsilon=0$ there is no region of decay separating the linearly damped and the resonant regions. Since both the Type I and the Type II energy exchange mechanisms operate simultaneously at all values of Ri_n, we conclude that with other parameters fixed the change from the linearly damped region to the resonant region involves only a gradual change in the relative magnitudes of the two mechanisms. In drawing the dashed line in question we presume that if a calculation had been carried out with slowly increasing Ri_n, the calculated wave would have shown a smooth variation of c across $\mathrm{Ri}_n=3$ even though the wave slowly decayed in that narrow interval of Ri_n.

6. Conclusions

1) For low values of the Richardson number the growth rates of instability of the Ekman boundary layer decrease linearly with Ri at a rate dependent upon angle and wavelength, and possibly upon the other parameters Re, H and P, as well. As a result the angle and wavelength of maximum instability will change with Ri. For low Ri the wavelengths and angles of maximum instability are close to those for the Type I Ekman instability and the energy exchange appears to be dominated by the Type I mechanism.

2) Instability may occur at significantly larger values of Ri because of resonance of the incipient instability with internal gravity waves. A tendency in this direction occurs when the speed of propagation of the instability is within the range of speeds permitted for internal gravity waves by the Brunt-Väisälä frequency and by advection. Resonance is favored for $\epsilon<15$ since propagation to the left of the geostrophic flow is most likely to produce resonance. With angles close to $\epsilon=0$ and long wavelengths, the energy transfer in this region is dominated by the Type II instability mechanism.

3) At certain values of Ri and at some levels, usually near the bottom boundary, the perturbation heat flux may be opposite in direction to that normally expected. In such cases negative heat transfer coefficients occur due to phase relations between temperature and vertical velocity forced by differential horizontal advection in the boundary layer. This condition could not be maintained in a finite-amplitude equilibrium.

4) Other hydrodynamic instabilities in which stratification is normally a damping influence may be affected in a similar way if the shear flow instability can propagate within the possible range of speeds of internal gravity waves. Brown (1972) has emphasized the importance of a cutoff of instability at a critical local Richardson number, $\mathrm{Ri}=1/4$, and the hydrodynamic literature is repleat with references to this limit. However, it should be noted that the theories leading to this criterion have not included the effects of rotation and we should not necessarily accept this limit for the present problem.

Table 2 clearly shows that at $\mathrm{Ri}_n=16$ and $\epsilon=0$ instability was found over a broad range of wavelengths. From Table 1 the corresponding local Richardson number at the inflection point is $\mathrm{Ri}_l=0.5685$, significantly exceeding 0.25. On the other hand, Ri (the local value at $z=0$) does not exceed 0.25 for any calculated case, and so there always was at least one part of the fluid in which the necessary condition for instability was satisfied. These considerations are consistent with the conclusion that the inflectional instability (Type I) is damped out with $\mathrm{Ri}_l<0.25$, but the parallel mode instability (Type II) is not. For the latter mechanism the value of Ri at $z=0$ is appropriate, but our calculations do not extend to sufficiently high Ri and Re to determine a limiting value of Ri for this problem.

5) With respect to atmospheric applications, the time scale for the growth of disturbances is given here in terms of the rotation rate of the coordinate system. Thus, a growth rate k corresponds to an e-folding time $t=24/(2\pi k \sin\psi)$ hours where ψ is latitude. For $k=1$, typical of maximum growth rates at $\mathrm{Ri}_n=8$ (see Table 2), $t=5.4$ hr at $\psi=45°$. A turbulent Reynolds number for the Ekman layer of the atmosphere may be defined by $\mathrm{Re}_t=U_g/(\nu_t\Omega\sin\psi)^{\frac{1}{2}}$ where ν_t is a vertically averaged turbulent viscosity, and for neutral stability $\mathrm{Re}_t\approx 600$ (Faller, 1965). But stable stratification probably increases Re_t by a reduction of ν_t, thus leading to larger values of k than have been computed here for $\mathrm{Re}=600$. Stratification would tend to preferentially dampen the larger scales of turbulence with the exception of the unstable modes as found here. Thus, whereas an unstratified boundary layer might exhibit a continuous spectrum of turbulence up to and including those scales characteristic of the unstable Ekman layer, a stratified layer may well retain only the smaller scale turbulence and the larger scale instability so as to exhibit a bi-modal energy spectrum.

6) Angell *et al.* (1969) reported the dominance of Brunt-Väisälä periods of oscillation in the stratified planetary boundary layer of the atmosphere. These oscillations probably represented internal waves, and the mechanism considered in this paper is one possible source of energy for such oscillations. To illustrate that this is a reasonable assertion we estimate Ri from the average conditions of Angell *et al.*, taking a turbulent Reynolds number as $\mathrm{Re}_t=\bar{U}/(D_t\Omega\sin\psi)$ and a turbulent Richardson number as $\mathrm{Ri}_t=g\Delta\bar{\theta}D_t^2/(\bar{U}^2\bar{\theta}\Delta Z')$, where $D_t=(\nu_t/\Omega\sin\psi)^{\frac{1}{2}}$ is the turbulent Ekman depth. With $\psi=37°$, $\bar{U}=5.1$ m sec^{-1}, $\bar{\theta}=300°$, $\Delta\bar{\theta}=0.13°$, $\Delta Z'=100$ m, and estimating $\mathrm{Re}_t=1000$, it follows that $D_t=117$ m and $\mathrm{Ri}_t=0.022$. From Table 1 this value is close to $\mathrm{Ri}_n=16$.

Table 2 and Fig. 9 suggest that a wavelength $L=26$ and a speed $c=0.32$ are appropriate for this value of Ri_n

although they were determined with Re=600 rather than Re=1000. Nevertheless, with these values of c and L the calculated nondimensional frequency at a fixed point is $\omega=77.4$, and the corresponding dimensional period of oscillation would be 31 min. For comparison at $\Delta\bar{\theta}/\Delta Z'=0.13$ deg (100 m)$^{-1}$ the Brunt-Väisälä period is 16 min.

More detailed estimates from individual sets of observations would require better estimates of the way in which stable stratification alters Re_t and therefore ν_t, D_t and Ri_t. Indeed, with the many complexities of the turbulent stratified boundary layer further speculation does not seem to be warranted at this time.

REFERENCES

Angell, J. K., D. H. Pack and N. Delver, 1969: Brunt-Väisälä oscillations in the planetary boundary layer. *J. Atmos. Sci.*, **26**, 1245–1252.

Brown, Robert A., 1972: The inflection point instability of a stratified Ekman boundary layer. *J. Atmos. Sci.*, (in press).

Burgers, J. M., 1953: Some considerations on turbulent flow with shear. *Proc. Netherlands Acad. Sci.*, **B56**, 125–147.

Eckart, C., 1960: *Hydrodynamics of Oceans and Atmospheres*. New York, Pergamon Press, 290 pp.

Faller, A. J., 1963: An experimental study of the instability of the laminar Ekman boundary layer. *J. Fluid Mech.*, **15**, 560–576.

——, 1965: Large eddies in the atmospheric boundary layer and their possible role in the formation of cloud rows. *J. Atmos. Sci.*, **22**, 176–184.

——, and R. Kaylor, 1966: A numerical study of the instability of the laminar Ekman boundary layer. *J. Atmos. Sci.*, **23**, 466–480.

——, and ——, 1967: Instability of the Ekman spiral with applications to the planetary boundary layers. *Phys. Fluids Suppl.*, IUGG-IUTAM Symposium, 19–24 September, Kyoto, Japan, S212–S219.

——, and ——, 1969: Instability of the thermal wind. *Clear Air Turbulence and Its Detection*, New York, Plenum Press, 542 pp.

Lilly, D. K., 1966: On the instability of Ekman boundary flow. *J. Atmos. Sci.*, **23**, 481–489.

Schlichting, H., 1960: *Boundary Layer Theory*, 4th ed. New York, McGraw-Hill, 647 pp.

Stone, P. H., 1966: On non-geostrophic baroclinic stability. *J. Atmos. Sci.*, **23**, 390–400

Tatro, P., and E. L. Mollo-Christensen, 1967: Experiments on Ekman layer instability. *J. Fluid Mech.*, **28**, 531–543.